JOURNAL OF APPLIED ELECTROCHEMISTRY 24 (1994) 361–367

Cyclic voltammetry at a metallic electrode: application to the reduction of nickel, tantalum and niobium salts in fused electrolytes

F. LANTELME, Y. BERGHOUTE, A. SALMI

Laboratoire d'Electrochimie, U.R.A. 430 CNRS, U.P.M.C., Case 51, 4 Place Jussieu, 75252 Paris, Cedex 05, France

Received 7 May 1993

Electrodeposition of metals was studied by linear sweep voltammetry at a metallic electrode. A mathematical analysis is available for reactions controlled by diffusion. A finite difference algorithm is presented for digital simulation of complex mechanisms comprising adsorption, multistep reaction and formation of a surface layer of insoluble compounds. It was used to study the deposition of tantalum and niobium from fused salts.

1. Introduction

The most noteworthy feature of commercial processes for electrowinning metal from molten salts is that they involve liquid metals (alkali and alkali-earth metals, aluminium) that are easily extracted from the cell after electrolytic production [1]. However, attempts have been made to electrodeposit metals in the solid form. In the past decades this effort has been oriented towards the preparation of the refractory metals (transition elements of groups IVa, Va and VIa of the periodic table). These metals are traditionally prepared by thermal reduction of their salts or oxides using a chemical agent such as carbon, sodium, magnesium, aluminium or calcium [2]. These processes do not always yield a sufficient purity and it is generally considered that the electrolytic route using fused electrolyte is a promising technique, which is also convenient for producing metal alloys [3], such as Ni_3Nb.

The mechanism of the electroreduction of refractory metals is not yet completely elucidated. This is due to the complexity of the electrochemical reactions. The variety of oxidation states existing in fused baths induces disproportionation reactions such as $5Ta^{4+} \rightarrow Ta + 4Ta^{5+}$ [1]. The metal deposition occurs through a multistep process including lower oxidation states. For niobium, four oxidation states are detected during the reduction of $NbCl_5$ dissolved in LiCl–KCl: Nb^{5+}, Nb^{4+}, Nb^{3+} and Nb^{2+}; moreover, complexed compounds, such as Nb_3Cl_8, appeared at the electrode surface [4]. These intermediate compounds, often sparingly soluble, remain adsorbed at the electrode surface and disturb the metal deposition.

To study the mechanism of the electrochemical reactions, the dissolution–deposition technique was used. This consists in performing a cyclic potential sweep at a working electrode made of a pure metal, M. During the anodic sweep, the metal ions are generated, $M \rightarrow M^{n+} + ne^-$; the reduction of the generated ions is studied during the backward sweep. A mathematical analysis of this process has been carried out for reversible reactions [5]. In the present work the analysis is illustrated on the model case of the redox reaction $Ni \rightarrow Ni^{2+} + 2e^-$. Perturbations arising from more complex mechanisms are studied by digital simulation. The influence of the concentration of electroactive ions is examined. Then, the behaviour of refractory metals, tantalum and niobium, is studied; the interpretation of the experiments requires a large extension of the previous analysis. Computer programs are designed to include the case of multistep reactions controlled by the electron transfer and involving adsorbed species.

2. Experimental details

The electrochemical cell consisted of an outer Pyrex or Hastelloy® (Cabot Corporation) envelope, at the base of which was the glassy carbon vessel containing the molten salt [6]. The experiments were carried out under argon atmosphere. The LiCl–KCl or NaCl–KCl eutectic mixture was purified according to a procedure involving high vacuum desiccation, chlorine bubbling, argon flushing electrolysis and filtering in a separate silica cell [7].

The reference electrode was a chlorine electrode [8] in LiCl–KCl, or a Ni^{2+}/Ni electrode (1 mol % $NiCl_2$) in NaCl–KCl; this last electrode was standardized by use of an internal reference system [9]. Wires of pure metal (Matthey Reagent), diameter 1 mm, were used as working and counter electrodes. For the generation of potential sweeps a Tacussel GSTP4 programmer and a Tacussel PRT 20/10 potentiostat were used. The voltammograms were obtained on a Sefram X–Y recorder, unless stored in a Nicolet 310

0021-891X

digital oscilloscope as an intermediate storage device.

3. Reversible reaction: $Ni^{2+} + 2e^- \Leftrightarrow Ni$

3.1. *Electrolyte without M^{n+} ions (nickel ions)*

The shape of the voltammogram reported in Fig. 1 is typical of a redox reaction, $M \rightarrow M^{n+} + ne^-$, involving the dissolution of an insoluble substance [5]. Two extreme values of the current density, i, are observed. The first, i_M, occurs at the most positive potential, E_M (right hand side of the potential window). The second, i_m, occurs at a potential, E_m, during the electroreduction of the freshly generated ions; this is due to ion depletion in the vicinity of the electrode. The theoretical analysis of the voltammogram for a diffusion controlled reaction was performed recently [5]. The current density, i_M, is given by

$$i_M = nF(D_1 nf\nu)^{1/2} \exp[nf(E_M - E_1^0)] \quad (1)$$

with $f = F/RT$; D_1 is the diffusion coefficient of M^{n+} species; ν is the sweep rate; E_1^0 is the standard potential of the redox couple. The solution of M^{n+} is assumed ideal, and the activity of the insoluble substance, here the pure metal, is equal to unity. The voltammogram is described by the two equations. For the forward step

$$i = i_M \exp[nf(E - E_M)] \quad (2)$$

and, for the reverse cycle

$$i = i_M\{\exp[-nf(E - E_M)]\,\mathrm{erfc}[-nf(E - E_M)]^{1/2} - 2\pi^{-1/2}\,\mathrm{Daw}[-nf(E - E_M)]^{1/2}\} \quad (3)$$

erfc is the complementary error function and Daw the Dawson integral [10] viz.

$$\mathrm{Daw}(z) = \exp(-z^2)\int_0^z \exp(u^2)\,du$$

The theory shows that the ratio of the two peak currents remains constant: $i_m/i_M = -0.194$. The separation of the two peak potentials is $E_m - E_M = -1.367/nf$. The experimental curves show that the ratio i_m/i_M obeys the previous theoretical relation with an accuracy of $\pm 8\%$ at any scan rate ($0.2 < \nu < 10\,V\,s^{-1}$).

The agreement between experimental and theoretical curves indicates that the reaction is rapid and controlled by diffusion. According to the theory, the voltammogram is characterized by

$$\chi = D_1^{1/2} \exp(-nfE_1^0) \quad (4)$$

Indeed, for given experimental conditions (ν, E_M), the voltammogram depends only on χ. From Equation 1,

$$\chi = i_M/nF(nf\nu)^{1/2} \exp(nfE_M) \quad (5)$$

If one of the two parameters, D_1 or E_1^0, is known, the experimental values of χ, deduced from Equation 5, allows the determination of the other parameter. Here, the literature value [11] has been taken

$$D_1 = D_{Ni} = 1.56 \times 10^{-3} \exp(-3573/T) \quad (6)$$

the diffusion coefficient is in $cm^2\,s^{-1}$ and T in Kelvin. It is found that $E_{Ni}^0 = E_1^0 = -1.120\,V$ vs Cl_2/Cl^- at 450 °C. The error in D_{Ni} is $\pm 10\%$. The experimental error in χ is about $\pm 8\%$, then, according to Equation 4, the error in E_1^0 is about $\pm 5\,mV$.

3.2. *Electrolyte containing M^{n+} ions*

The presence of a non-negligible amount of Ni^{2+} causes the ratio, i_m/i_M, to increase as shown in Fig. 2. The boundary condition, $c_1(x, 0) = 0\,\forall x$, used to derive Equations 2 and 3, is no longer fulfilled. Digital simulation was used to interpret the experimental results. The concentration, $c_1(0, t)$, at the electrode surface obeys the Nernst equation

$$c_1(0, t) = \exp[nf(E(t) - E_1^0)] \quad (7)$$

with

$$E(t) = E_i + \nu t - 2\nu(t - t_M)H(t - t_M) \quad (8)$$

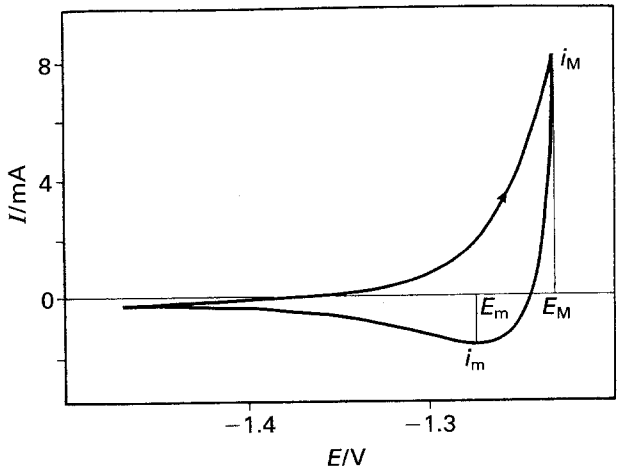

Fig. 1. Voltammogram for the reaction $Ni^{2+} + 2e^- \Leftrightarrow Ni$ at a nickel electrode (electrode area, $0.314\,cm^2$) in a LiCl–KCl eutectic mixture. $T = 402$ °C. Sweep rate: $0.24\,V\,s^{-1}$. Reference electrode: Cl_2/Cl^-.

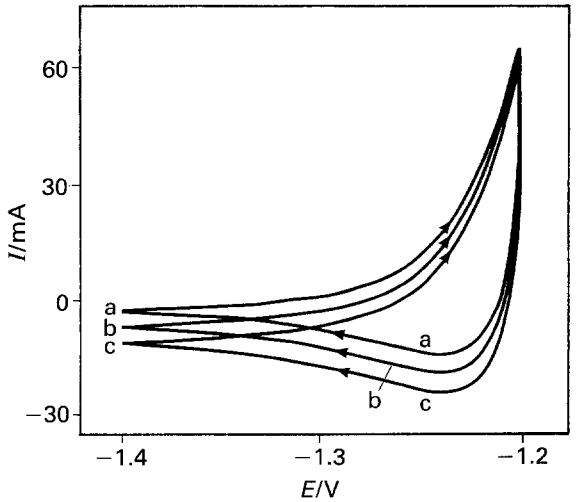

Fig. 2. Voltammograms for the reaction $Ni^{2+} + 2e^- \Leftrightarrow Ni$ at a nickel electrode (electrode area, $1\,cm^2$) in a LiCl–KCl eutectic mixture. $T = 400$ °C. Sweep rate: $1\,V\,s^{-1}$. Reference electrode: Cl_2/Cl^-. Concentration of Ni^{2+} (10^{-3} mol dm^{-3}): (a) 0.03, (b) 13, (c) 22.

E_i is the initial potential, t_M is the time of the reversal of the linear potential sweep and H the unit step function. The concentration profile in the electrolyte is calculated from the finite difference technique. The space (the x coordinate) was divided into small intervals of length Δx and time into small time steps, Δt. The concentration $c_1(x, t+\Delta t)$ is given by the recursive relation [12]

$$c_1(x,t+\Delta t) = c_1(x,t) + \frac{D_1 \Delta t}{\Delta x^2}[c_1(x-\Delta x,t) - 2c_1(x,t) + c_1(x+\Delta x,t)] \quad (9)$$

The current density is calculated from the concentration gradient at the electrode surface

$$i = nFD_1 \frac{c_1(0,t) - c_1(\Delta x,t)}{\Delta x} \quad (10)$$

The $i = f(E)$ curve is deduced by an iterative process using Equations 7 and 9. The parameter E_1^0 is adjusted according to a least squares procedure to obtain the best fit with the experimental curve. Voltammograms for increasing amounts of Ni^{2+} are shown in Fig. 2. The value of E_{Ni}^0 obeys the equation

$$E_{Ni}^0 = -1.410 + 0.415 \times 10^{-3} T \quad (11)$$

where T is in kelvin.

Within the range of accuracy of the experimental determinations (± 5 mV), these values are in good agreement with previous e.m.f. measurements [13].

Concerning the electrochemical reactions at a working electrode of a refractory metal, preliminary experiments have shown that the reaction involves a multistep electron transfer and adsorption phenomena [14]. The procedure used for studying the reaction is now described.

4. Charge-transfer kinetics, fundamental analysis

4.1. *One step reaction*

Consider the reaction

$$M \Longleftrightarrow M^{n1+} + n_1 e^- \quad (12)$$

The current is related to the overpotential, η, by [15]

$$i_1 = i_{10}^0 \left\{ \exp[\alpha_1 n_1 f\eta(t)] - \frac{c_1(0,t)}{c_1^*} \times \exp[-(1-\alpha_1) n_1 f\eta(t)] \right\} \quad (13)$$

where c_1^* is the bulk concentration of M^{n1+}, α_1 is the transfer coefficient, and i_{10}^0 the exchange current density. Substituting $\eta(t+\Delta t)$ for $\eta(t)$ and equating the two expressions for the current (Equations 13 and 10 with $n = n_1$ and $i = i_1$) yields

$$c_1(0,t+\Delta t) = \frac{\left[\frac{i_{10}^0}{n_1} \exp[\alpha_1 n_1 f\eta(t+\Delta t) + \frac{FD_1}{\Delta x} c_1(\Delta x,t)\right]}{\left[\frac{i_{10}^0}{n_1 c_1^*} \exp[-(1-\alpha_1) n_1 f\eta(t+\Delta t)] + \frac{FD_1}{\Delta x}\right]} \quad (14)$$

The concentration profile is calculated from Equation 9, and the current from Equation 10 or 13. To simulate a sweep (forward and backward) the total number of iterations was typically 5000.

4.2. *Multistep reaction*

Consider now the model case of a three-step reaction

$$\{ \quad 1 \qquad 2 \qquad 3$$

The electron flows related to steps 1 and 2 are given by the current–overpotential equations

$$i_1 = i_{10}^0 \left\{ \exp[\alpha_1 n_1 f\eta(t)] - \frac{c_1(0,t)}{c_1^*} \exp[-(1-\alpha_1) n_1 f\eta(t)] \right\} \quad (16)$$

and

$$i_2 = i_{21}^0 \left\{ \frac{c_1(0,t)}{c_1^*} \exp[\alpha_2 n_2 f\eta(t)] - \frac{c_2(0,t)}{c_2^*} \exp[-(1-\alpha_2) n_2 f\eta(t)] \right\} \quad (17)$$

The concentrations of $M^{(n1+n2)+}$ and $M^{(n1+n2+n3)+}$ obey the Nernst law

$$c_3(0,t) = c_2(0,t) \exp[n_3 f(E(t) - E_{32}^0)] \quad (18)$$

The material balances for M^{n1+} and $M^{(n1+n2)+}$ during electrolysis give

$$\frac{i_1}{n_1 F} - \frac{i_2}{n_2 F} = D_1 \frac{c_1(0,t) - c_1(\Delta x,t)}{\Delta x} \quad (19)$$

$$\frac{i_2}{n_2 F} = D_2 \frac{c_2(0,t) - c_2(\Delta x,t)}{\Delta x} + D_3 \frac{c_3(0,t) - c_3(\Delta x,t)}{\Delta x} \quad (20)$$

Substitution of the expressions for i_2 and $c_3(0,t)$ (Equations 17 and 18) into Equation 20 yields

$$c_2(0,t) = \boldsymbol{A} + \boldsymbol{B} c_1(0,t) \quad (21)$$

with

$$\boldsymbol{A} = \frac{n_2 F}{\Delta x}[D_2 c_2(\Delta x,t) + D_3 c_3(\Delta x,t)]/\boldsymbol{D} \quad (22)$$

$$\boldsymbol{B} = \frac{i_{21}^0}{c_1^*} \exp[\alpha_2 n_2 f\eta(t)]/\boldsymbol{D} \quad (23)$$

and

with

$$A = \frac{n_2 F}{\Delta x}[D_2 c_2(\Delta x, t) + D_3 c_3(\Delta x, t)]/D \quad (22)$$

$$B = \frac{i_{21}^0}{c_1^*}\exp[\alpha_2 n_2 f\eta(t)]/D \quad (23)$$

and

$$D = \frac{i_{21}^0}{c_2^*}\exp[-(1-\alpha_2)n_2 f\eta(t)] + \frac{n_2 F}{\Delta x}[D_2 + D_3 \exp[n_3 f(E(t) - E_{32}^0)]] \quad (24)$$

Substitution of the expressions for i_1 and i_2 (Equations 16 and 17) into Equation 19 provides

$$c_1(0,t) = N/M \quad (25)$$

with

$$N = n_2 i_{10}^0 \exp[\alpha_1 n_1 f\eta(t)] + n_1 n_2 F D_1 \frac{c_1(\Delta x, t)}{\Delta x} + n_1 n_2 F D_2 \frac{c_2(\Delta x, t) - A}{\Delta x} + n_1 n_2 F D_3 \frac{c_3(\Delta x, t) - A\exp[n_3 f(E(t) - E_{32}^0)]}{\Delta x} \quad (26)$$

and

$$M = \frac{n_2 i_{10}^0}{c_1^*}\exp[-(1-\alpha_1)n_1 f\eta(t)] + n_1 n_2 F\frac{D_1}{\Delta x} + n_1 n_2 F B\frac{D_2}{\Delta x} + n_1 n_2 F B\frac{D_3}{\Delta x}\exp[n_3 f(E(t) - E_{32}^0)] \quad (27)$$

The concentrations at $t + \Delta t$ are calculated from Equations 25, 21 and 18, $E(t + \Delta t)$ and $\eta(t + \Delta t)$ being substituted for $E(t)$ and $\eta(t)$ (Equations 16–27). The concentration profiles of M^{n1+}, $M^{(n1+n2)+}$ and $M^{(n1+n2+n3)+}$ are calculated from recursive relations (Equation 9). The current flowing through the cell is

$$i = n_1 F D_1 \frac{c_1(0,t) - c_1(\Delta x, t)}{\Delta x} + (n_1 + n_2) F D_2 \frac{c_2(0,t) - c_2(\Delta x, t)}{\Delta x} + (n_1 + n_2 + n_3) F D_3 \frac{c_3(0,t) - c_3(\Delta x, t)}{\Delta x} \quad (28)$$

4.3. *Multistep reaction with adsorption*

Consider again the scheme 15. It is assumed that the surface concentration of adsorbed M^{n1+} and $M^{(n1+n2)+}$ obeys a simplified Langmuir equation

$$\Gamma_1(t) = k_1 c_1(0,t) \quad (29)$$

and

$$\Gamma_2(t) = k_2 c_2(0,t) \quad (30)$$

Taking account of the amounts of adsorbed species, the material balances for M^{n1+} and $M^{(n1+n2)+}$ take the form

$$\frac{i_1}{n_1 F} - \frac{i_2}{n_2 F} = D_1 \frac{c_1(0,t) - c_1(\Delta x, t)}{\Delta x} + k_1 \frac{c_1(0,t) - c_1(0, t - \Delta t)}{\Delta t} \quad (31)$$

$$\frac{i_2}{n_2 F} = D_2 \frac{c_2(0,t) - c_2(\Delta x, t)}{\Delta x} + D_3 \frac{c_3(0,t) - c_3(\Delta x, t)}{\Delta x} + k_2 \frac{c_2(0,t) - c_2(0, t - \Delta t)}{\Delta t} \quad (32)$$

Following the same procedure as previously gives

$$c_1(0,t) = N'/M' \quad (33)$$

with

$$N' = N + \frac{n_1 n_2 F}{\Delta t}\{k_1 c_1(0, t - \Delta t) + k_2[c_2(0, t - \Delta t) - A]\} \quad (34)$$

$$M' = M + n_1 n_2 F\frac{k_1}{\Delta t} + n_1 n_2 F\frac{k_2}{\Delta t}B \quad (35)$$

The concentration $c_1(0, t + \Delta t)$ is calculated from Equation 33 by substituting $E(t + \Delta t)$ and $\eta(t + \Delta t)$ for $E(t)$ and $\eta(t)$. Then, $c_2(0, t + \Delta t)$ is calculated from

$$c_2(0, t + \Delta t) = A' + B' c_1(0, t + \Delta t) \quad (36)$$

with

$$A' = n_2 F\left[\frac{D_2 c_2(\Delta x, t)}{\Delta x} + \frac{D_3 c_3(\Delta x, t)}{\Delta x} + \frac{k_2 c_2(0, t - \Delta t)}{\Delta t}\right]/D' \quad (37)$$

$$B' = \frac{i_{21}^0}{c_1^*}\exp[\alpha_2 n_2 f\eta(t + \Delta t)]/D' \quad (38)$$

and

$$D' = \frac{i_{21}^0}{c_2^*}\exp[-(1-\alpha_2)n_2 f\eta(t + \Delta t)] + n_2 F \times \left[\frac{D_2}{\Delta x} + \frac{D_3 \exp[n_3 f(E(t + \Delta t) - E_{32}^0)]}{\Delta x} + \frac{k_2}{\Delta t}\right] \quad (39)$$

The concentration $c_3(0, t + \Delta t)$ is given by the Nernst equation

$$c_3(0, t + \Delta t) = c_2(0, t + \Delta t) \times \exp[n_3 f(E(t + \Delta t) - E_{32}^0)] \quad (40)$$

The concentration profiles of M^{n1+}, $M^{(n1+n2)+}$ and $M^{(n1+n2+n3)+}$ are calculated from Equation 9. The

current flowing through the cell is

$$i = n_1F\left[D_1\frac{c_1(0,t)-c_1(\Delta x,t)}{\Delta x} + k_1\frac{c_1(0,t)-c_1(0,t-\Delta t)}{\Delta x}\right] + (n_1+n_2)F\left[D_2\frac{c_2(0,t)-c_2(\Delta x,t)}{\Delta x} + k_2\frac{c_2(0,t)-c_2(0,t-\Delta t)}{\Delta t}\right] + (n_1+n_2+n_3)FD_3\frac{c_3(0,t)-c_3(\Delta x,t)}{\Delta x} \quad (41)$$

4.4. *Multistep reaction with formation of a layer of cluster compounds*

A layer of insoluble cluster compounds often appears at the metal/electrolyte interface. This consists of salts at low oxidation states. For solutions of niobium chlorides, compounds such as Nb_3Cl_8 or Nb_6Cl_{14} have been detected [16]. This situation is described by the scheme

$$\overbrace{}^{\text{species}}$$
$$1 \qquad 2 \qquad 3$$
$$\mathrm{M} \underset{\text{slow}}{\overset{n_1e^-}{\Longleftrightarrow}} \underset{\substack{\text{surface}\\ \text{layer}}}{\mathrm{M}^{n1+}} \underset{\text{slow}}{\overset{n_2e^-}{\Longleftrightarrow}} \mathrm{M}^{(n1+n2)+} \underset{\text{rapid}}{\overset{n_3e^-}{\Longleftrightarrow}} \mathrm{M}^{(n1+n2+n3)+}$$
$$\underbrace{}_{\text{step}}$$
$$1 \qquad 2 \qquad 3 \quad (42)$$

It is assumed that the maximum number of moles of M^{n1+} per surface unit of layer is G_M. The electron flows associated with steps 1 and 2 are given by

$$i_1 = i_{10}^0\left\{\left(\frac{1-G_1(t)/G_M}{1-G_1^*/G_M}\right)\exp\left[\alpha_1 n_1 f\eta(t)\right] - \frac{G_1(t)}{G_1^*}\exp\left[-(1-\alpha_1)n_1 f\eta(t)\right]\right\} \quad (43)$$

and

$$i_2 = i_{21}^0\left\{\frac{G_1(t)}{G_1^*}\exp\left[\alpha_2 n_2 f\eta(t)\right] - \left(\frac{1-G_1(t)/G_M}{1-G_1^*/G_M}\right)\frac{c_2(0,t)}{c_2^*} \times \exp\left[-(1-\alpha_2)n_2 f\eta(t)\right]\right\} \quad (44)$$

where $G_1(t)$ is the number of moles of M^{n1+} per unit surface of layer.

Considering the mass balances of M^{n1+} and $M^{(n1+n2)+}$ during the electrolysis shows that $c_2(0,t+\Delta t)$ obeys the equation

$$N''[c_2(0,t+\Delta t)]^2 + M''c_2(0,t+\Delta t) - L'' = 0 \quad (45)$$

with

$$N'' = \frac{i_{21}^0}{G_M c_2^*(1-G_1^*/G_M)}B'' \times \exp\left[-(1-\alpha_2)n_2 f\eta(t+\Delta t)\right] \quad (46)$$

$$M'' = \frac{i_{21}^0}{c_2^*}\left(\frac{1-A''/G_M}{1-G_1^*/G_M}\right)\exp\left[-(1-\alpha_2)n_2 f\eta(t+\Delta t)\right] + \frac{i_{21}^0}{G_1^*}B''\exp\left[\alpha_2 n_2 f\eta(t+\Delta t)\right] + \frac{n_2F}{\Delta x}\left[D_2 + D_3\exp\left[n_3 f(E(t+\Delta t)-E_{32}^0)\right]\right] \quad (47)$$

$$L'' = \frac{i_{21}^0}{G_1^*}A''\exp\left[\alpha_2 n_2 f\eta(t+\Delta t)\right] + \frac{n_2F}{\Delta x}\left[D_2c_2(\Delta x,t) + D_3c_3(\Delta x,t)\right] \quad (48)$$

and

$$G_1(t+\Delta t) = A'' - B''c_2(0,t+\Delta t) \quad (49)$$

with

$$A'' = \left\{\frac{i_{10}^0}{n_1(1-G_1^*/G_M)}\exp\left[\alpha_1 n_1 f\eta(t+\Delta t)\right] + \frac{F}{\Delta x}\left[D_2c_2(\Delta x,t) + D_3c_3(\Delta x,t)\right] + \frac{F}{\Delta t}G_1(t)\right\}/C'' \quad (50)$$

$$B'' = \frac{F}{\Delta x}\left[D_2 + D_3\exp\left[n_3 f(E(t+\Delta t)-E_{32}^0)\right]\right]/C'' \quad (51)$$

$$C'' = \frac{i_{10}^0}{n_1G_M(1-G_1^*/G_M)}\exp\left[\alpha_1 n_1 f\eta(t+\Delta t)\right] + \frac{i_{10}^0}{n_1G_1^*}\exp\left[-(1-\alpha_1)n_1 f\eta(t+\Delta t)\right] + \frac{F}{\Delta t} \quad (52)$$

The concentration $c_2(0,t+\Delta t)$ is given by the positive root of Equation 45; $G_1(t+\Delta t)$ and $c_3(0,t+\Delta t)$ are calculated from Equations 49 and 40, respectively. The current density is given by

$$i = n_1F\frac{G_1(t+\Delta t)-G_1(t)}{\Delta t} + (n_1+n_2)FD_2\frac{c_2(0,t+\Delta t)-c_2(\Delta x,t+\Delta t)}{\Delta x} + (n_1+n_2+n_3)FD_3\frac{c_3(0,t+\Delta t)-c_3(\Delta x,t+\Delta t)}{\Delta x} \quad (53)$$

5. Experimental results

5.1. *Tantalum: a multistep reaction with adsorption*

It has been pointed out that Ta^{2+}, Ta^{4+} and Ta^{5+} species are stable in LiCl–KCl and insoluble

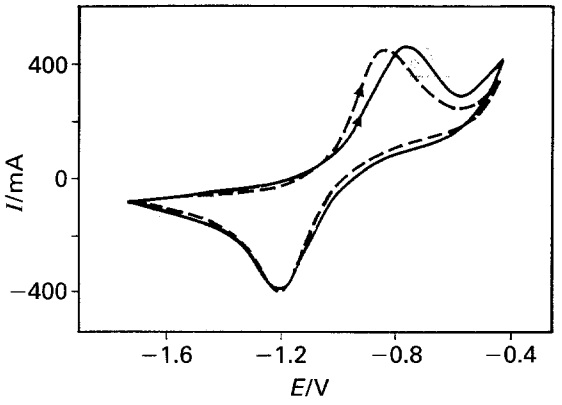

Fig. 3. Voltammogram at a tantalum electrode (electrode area: 0.314 cm^2) in a LiCl–KCl eutectic mixture. $T = 450\,°C$. Sweep rate: 0.324 $V\,s^{-1}$. Reference electrode: Cl_2/Cl^-. Full line: experimental. Dashed line: simulated.

compounds can appear at the surface of the electrode [17, 18]. A typical voltammogram at a tantalum electrode is shown in Fig. 3. The steep peak at the right hand side of the picture is the wall of oxidation of the metal. The two other peaks are due to the oxidation and reduction of compounds present at the electrode surface. The following scheme was used to interpret the experimental results

$$Ta \overset{2e^-}{\Longleftrightarrow} Ta^{2+} \overset{2e^-}{\Longleftrightarrow} Ta^{4+} \qquad (54)$$

The calculation was performed assuming that the two species, Ta^{2+} and Ta^{4+} behave as adsorbed species (Section 4.3). Preliminary calculations showed that the adsorption constants k_1 and k_2 were similar. To simplify the calculations it was assumed that they were equal. The parameters for the calculation are the standard potential and the rate constants [15] for the systems Ta^{2+}/Ta (E^0_{10}, k^0_{10}), Ta^{4+}/Ta^{2+} (E^0_{21}, k^0_{21}), and the adsorption constant. It was assumed that $\alpha_1 = \alpha_2 = 0.5$. The parameters were varied to obtain a calculated curve which fits the experimental curve (Fig. 3). The value of the standard potential at 450 °C, $E^0_{10} = -1.38$ V vs Cl_2/Cl^- (Table 1), is in good agreement with the value, $E^0_{10} = -1.39$ V, given by Picard *et al.* [19]. The value of the adsorption constant indicates that in the potential range of the experiments the amount of adsorbed species is about $10^{-6}\,mol\,cm^{-2}$. A large part of the current comes from the oxidation and reduction of the adsorbed species giving rise to two peaks during the potential sweep (Fig. 3).

At high temperature (720 °C) in NaCl–KCl, it has been shown that tantalum oxidizes directly to Ta^{5+}

Table 1. Standard potentials, E^0_{10}, E^0_{21} (molarity scale), and kinetic constants, k^0_{10}, k^0_{21}, for the reactions $Ta \Leftrightarrow Ta^{2+} + 2e^-$ and $Ta^{2+} \Leftrightarrow Ta^{4+} + 2e^-$ in LiCl–KCl. Reference electrode: chlorine electrode. k_a, adsorption constant

T /°C	E^0_{10} /V	E^0_{21} /V	$10^{12} \times k^0_{10}$ /cm s^{-1}	$10^3 \times k^0_{21}$ /cm s^{-1}	$10^4 \times k_a$ /cm
380	−1.398	−1.042	1.6	3.7	0.88
450	−1.377	−1.019	24.8	6.2	4.4
496	−1.362	−1.003	124	8.3	11

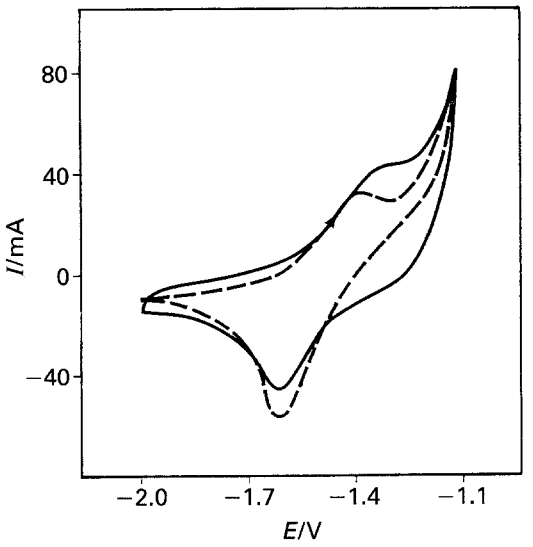

Fig. 4. Voltammogram at a niobium electrode (electrode area: 0.314 cm^2) in a LiCl–KCl eutectic mixture. $T = 550\,°C$. Sweep rate: 0.885 $V\,s^{-1}$. Reference electrode: Cl_2/Cl^-. Full line: experimental. Dashed line: simulated.

[20]. However, at a tantalum electrode, two bumps are visible before the oxidation wall of the metal (Fig. 6 in [20]). These bumps are attributed to the presence of the transient formation of a thin layer of adsorbed compounds.

5.2. *Voltammetry at a niobium electrode*

Voltammograms at a niobium electrode are shown in Figs 4 and 5. The bump before the wall current of the oxidation of the metal is due to the presence of a layer of niobium subhalides at the electrode surface. Previous research has shown that Nb^{3+} and Nb^{4+} species were stable in the alkali chloride melts [4]. The present work indicates that an intermediate step occurs at the electrode surface involving a variable amount of subhalide clusters [16]. For niobium the scheme 15 is written

$$Nb \overset{2e^-}{\Longleftrightarrow} \underset{\text{layer}}{Nb^{2+}} \overset{e^-}{\Longleftrightarrow} Nb^{3+} \overset{e^-}{\Longleftrightarrow} Nb^{4+} \qquad (55)$$

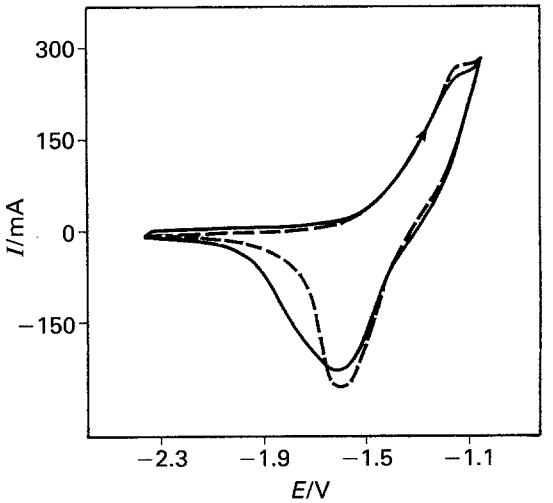

Fig. 5. Voltammogram at a niobium electrode (Electrode area: 0.32 cm^2) in a NaCl–KCl eutectic mixture. $T = 700\,°C$. Sweep rate: 1 $V\,s^{-1}$. Reference electrode: Cl_2/Cl^-. Full line: experimental. Dashed line: simulated

Table 2. Standard potentials, E_{10}^0, E_{21}^0 (molarity scale), and kinetic constants, k_{10}^0, k_{21}^0, for the reactions $Nb \Leftrightarrow Nb^{2+}_{(layer)} + 2e^-$ and $Nb^{2+}_{(layer)} \Leftrightarrow Nb^{3+} + e^-$. Reference electrode: chlorine electrode. G_M: mole of Nb^{2+} in the surface layer. E^*, equilibrium potential; c^*_{Nb3+}, equilibrium concentration, calculated value, E_3^0, for the couple Nb^{3+}/Nb

T /°C	E^* /V	$10^6 \times c^*_{Nb3+}$ /mol cm^{-3}	E_{10}^0 /V	E_{21}^0 /V	E_3^0 /V	$10^6 \times k_{10}^0$ /cm s^{-1}	$10^4 \times k_{21}^0$ /cm s^{-1}	$10^8 \times G_M$ /mol cm^{-2}
LiCl–KCl								
445	−1.594	0.17	−1.542	−1.161	−1.415	0.93	0.12	5.8
498	−1.564	0.25	−1.500	−1.140	−1.380	8.2	1.6	9.7
550	−1.498	2	−1.478	−1.097	−1.351	19.5	3.4	8.1
NaCl–KCl								
670	−1.360	116	−1.380	−1.146	−1.302	68	8.0	140
700	−1.576	0.03	−1.401	−1.056	−1.286	52	10	81

The calculation was performed according to the model of Section 4.4. It was assumed that $\alpha_1 = \alpha_2 = 0.5$. The parameters for the calculation are the standard potential and the rate constants for the systems Nb^{2+}/Nb (E_{10}^0, k_{10}^0), Nb^{3+}/Nb^{2+} (E_{21}^0, k_{21}^0) and the amount of Nb^{2+}. The value of the standard potential of the reversible reaction Nb^{4+}/Nb^{3+} was taken from literature data [4, 21]. The parameters were varied to obtain a calculated curve which fits the experimental curve.

The standard potential, E_3^0 for the Nb^{3+}/Nb couple is in very good agreement with previous determination [4]. The results (Table 2) show that a higher temperature induces a large positive shift in the standard potentials of both systems Nb^{2+}/Nb and Nb^{3+}/Nb^{2+}. This trend is in good agreement with previous experiments [4]. It seems that the composition of the electrolyte does not significantly affect the value of the standard potential, E_3^0; in LiCl–KCl the value, $E_3^0 = -1.3$ V vs Cl_2/Cl^-, has been reported at 620 °C [4]. E_3^0 obeys the equation

$$E_3^0 = -1.77 + 0.505 \times 10^{-3} T \qquad (56)$$

with temperature T in kelvin.

A higher temperature induces a large increase in the kinetic constants k_{10}^0 and k_{21}^0 (within the range of accuracy of the measurement, ±30%). The faster reaction rate suggests why the metal deposition was easier and less perturbed by the presence of subhalides at high temperature [4].

6. Conclusion

The dissolution–deposition technique appears to be an efficient and simple tool for studying the mechanism of metal electrodeposition. Only rods of pure metal are required, the corresponding ions being generated by anodic dissolution. For reversible reactions controlled by the diffusion of ionic species, the experiments are interpreted within the frame of a mathematical analysis.

A finite difference algorithm was used for digital simulation of more complex mechanisms, comprising adsorption, multistep reaction, and formation of a surface layer of insoluble compounds. The treatment proves to be useful for examining the electrodeposition of refractory metals from fused salts. These metals such as niobium or tantalum exist at various oxidation states in the fused bath and cluster compounds form at the electrode surface which perturbs the metal deposition. The present work allows determination of the kinetics of the various reactions steps, and opens the way to a better understanding of electrocrystallization phenomena and deposition under pulsed regimes.

References

[1] D. Inman and S. H. White, *in* 'Molten Salt Electrolysis Production', International Symposium, Grenoble (1977), Institution of Mining and Metallurgy, London, p. 51.

[2] T. Rosenqvist, 'Principles of Extractive Metallurgy', McGraw-Hill, New York (1974) p. 426.

[3] A. Barhoun, F. Lantelme, M. E. de Roy and J. P. Besse, *Materials Science Forum* **73–75** (1991) 313.

[4] F. Lantelme, A. Barhoun and J. Chevalet, *J. Electrochem. Soc.* **140** (1993) 324.

[5] F. Lantelme and E. Cherrat, *J. Electroanal. Chem.* **244** (1988) 61.

[6] F. Lantelme, D. Inman and D. G. Lovering, *in* 'Molten Salt Techniques' (edited by R. J. Gale and D. G. Lovering), Plenum Press, New York (1984) Vol. 2, p. 181.

[7] T. Vargas and D. Inman, *J. Appl. Electrochem.* **17** (1987) 270.

[8] F. Lantelme, H. Alexopoulos, D. Devilliers and M. Chemla, *J. Electrochem. Soc.* **138** (1991) 1665.

[9] Y. Berghoute, A. Salmi and F. Lantelme, *J. Electroanal. Chem.*, in press.

[10] M. Abramowitz and I. A. Stegun, *in* 'Handbook of Mathematical Functions', 9th edn, Dover Publications, New York (1972) p. 319.

[11] G. J. Janz, C. B. Allen, N. P. Bansal, R.M. Murphy and R. P. T. Tomkins, *in* 'Physical Properties Data Compilations Relevant to Energy Storage', *NSRD-NBS 61*, Part II (1979) p. 232.

[12] D. Britz, 'Digital Simulation in Electrochemistry', Springer, Berlin (1988).

[13] F. Lantelme, J-F. Equey, S. Müller and M. Chemla, *J. Phys. Chem.* **95** (1991) 905.

[14] L. Arurault, J. Bouteillon, J. de Lepinay, A. Khalidi and J. C. Poignet, *Materials Science Forum* **73–75** (1991) 305.

[15] A. J. Bard and L. R. Faulkner, 'Electrochemical Methods', John Wiley, New York (1980).

[16] S. A. Kuznetsov, A. G. Morachevskii and P. T. Stangrit, *Soviet Electrochem.* **18** (1982) 1387.

[17] L. P. Polyakova, E. G. Polyakov, A. I. Sorokin and P. T. Stangrit, *J. Appl. Electrochem.* **22** (1992) 628.

[18] D. Brown, 'Comprehensive Chemistry', Vol. 3, Pergamon Press, Oxford (1973) p. 553.

[19] G. Picard, D. Ferry and P. Bocage, 'Rapport d'Activité du PIRSEM', Vol. III (1987) p. 229.

[20] F. Lantelme, A. Barhoun, G. Li and J.-P. Besse, *J. Electrochem. Soc.* **139** (1992) 1249.

[21] A. Barhoun, Y. Berghoute and F. Lantelme, *J. Alloys Compd.* **179** (1992) 241.